June. 2015. Vol. 7. No. 01 ISSN2305-8269
International Journal of Engineering and Applied Sciences

www.eaas-journal.org

LOCAL AND GLOBAL APPROACHES TO FRACTURE MECHANICS USING ISOGEOMETRIC ANALYSIS METHOD

[1*]ABDOLGHAFOOR KHADEMALRASOUL, [2]REZA NADERI

[1]Ph.D. Student., Department of Civil Engineering, Shahroud University of Technology, Iran.
[2] Asstt Prof., Department of Civil Engineering, Shahroud University of Technology, Iran.
E-mail: [1]ag.khadem@yahoo.com, [2]rz_naderi@yahoo.com

ABSTRACT

In the present research, implementations of different computational geometry technologies in isogeometric analysis framework for computational fracture mechanics are investigated. NURBS and T-splines are two different computational geometry technologies which are studied in this work. Among features of B-spline basis functions the possibility of enhancing a B-spline basis with discontinuities by means of knot insertion makes isogeometric analysis method a suitable candidate for modeling discrete cracks. Also repetition of two different control points between two patches can create a discontinuity and also demonstrates a singularity in the stiffness matrix. In the case of a pre-defined interface, non-uniform rational B-splines are used to obtain an efficient discretization. T-splines are a kind of computational geometry technology with the possibility of local refinement and also with no topologically rectangular arrangement of control points. Therefore, T-splines can decrease superfluous control points which they do not have any major effects on the geometry. Various numerical simulations demonstrate the suitability of the isogeometric analysis approach to fracture mechanics.

Keywords: ***Fracture mechanics, Isogeometric analysis method, Knot insertion, NURBS, T-splines.***

1. INTRODUCTION

Problems of fracture mechanics and numerical methods have attracted the attention of many prominent researchers over the years. In addition, integration between both of them has been interesting for researchers. However, material imperfections that arise at the time of production or usage of the material are unavoidable, and hence must be taken into account. Therefore, analysis of a cracked body is very crucial for engineers. In spite of progress of mesh generators, initial creation of the mesh with a strong discontinuity remains extremely heavy and difficult [1-3]. On the other hand, simultaneously with the further development of engineering complex designs, generating of exact geometries is required. Since the finite element mesh is only an approximation of the CAD (Computer Aided Design) geometry, which we will view as "exact", can create errors in many situations in analytical results [4]. Among the various numerical methods, only the isogeometric analysis approach (IGA) which utilizes NURBS as approximation basis functions can create an exact geometry [5, 6]. In fact, in the isogeometric analysis method the barrier between engineering design and analysis is broken down [7]. Therefore, using isogeometric analysis in fracture mechanics would be important to have the minimum amount of manipulating in the physical space in the whole of the process.

As a matter of fact, the possibility of continuity control in NURBS-based isogeometric analysis has become the IGA a capable approach in fracture mechanics and also in the cohesive zone modeling. Since NURBS-based isogeometric analysis method possesses unique computational properties, so, it is possible to create different types of discontinuities by using these facilities. Unlike partition of unity methods IGA facilitates modeling of discrete cracks and cohesive zones without additional evolutions in the physical space or performing a special mathematical formulation in the solution space. Hence, this analysis method may be attractive for engineers. On the other hand, the isogeometric analysis method can create the discontinuities by using its mathematical abilities. However, these inherent properties of the isogeometric analysis led us to use this method in computational fracture mechanics.

In this contribution, both NURBS (Non-Uniform Rational B-splines) and T-splines as two different computational geometry technologies are implemented in the isogeometric analysis

framework. Various studies have demonstrated that NURBS and T-splines have the same computational efficiencies [7-9].

The remainders of this paper are as follows. First in the rest of Section 1 the main topics on isogeometric analysis, NURBS and T-splines are discussed. The principles of fracture mechanics are explained in Section 2. Section 3 introduces the major concept of discontinuity creating in B-splines basis functions. Section 4 introduces the discretization concept in the isogeometric analysis method. Also the numerical simulations for 2D & 3D problems are studied in Section 5. Discretization of solid using T-splines is studied in Section 6. Finally, conclusions are summarized in Section 7.

1.1 Isogeometric Analysis Method

Isogeometric analysis method has emerged as an important alternative to traditional engineering design and analysis methodologies. Isogeometric analysis was introduced in [6] and later described in detail in [5]. In isogeometric analysis, the smooth geometric basis is used as the basis for analysis. Most of the early development in isogeometric analysis focused on establishing the behavior of the smooth NURBS basis in analysis. It was demonstrated that smoothness offers important computational advantages over standard finite elements [10-12]. Areas of application of isogeometric analysis include turbulence [13-15], fluid-structure interaction [16], structural analysis [11, 12], shape optimization [17, 18]. In reality, in the isogeometric analysis context the heavy and time consuming process of generation of the finite element mesh is vanished. Among the available finite element technologies for capturing discontinuities are interface elements [19, 20], and embedded discontinuities [21, 22]. Nowadays, the partition of unity method (PUM or X-FEM, [23-25]) is considered as the most flexible element technology for capturing propagating cracks. One possibility of discretizing the cohesive zone formulation using isogeometric finite elements is to use them in combination with the partition of unity method. In that case the discontinuities would be embedded in the solution space by means of Heaviside functions. Although such an approach would benefit from both advantages of the isogeometric approach, isogeometric finite elements offer the possibility to directly insert discontinuities in the solutions space. The conceptual idea is that in the isogeometric approach the inter element continuity can be decreased by means of knot insertion, e.g. [16]. In fact we can create a strong discontinuity or cohesive zone by using inherent specifications of NURBS basis functions. In addition to increasing the multiplicities of knot values in the parametric space, we can create a strong discontinuity in the physical domain with the repeated control points between two patches with identical coordinates.

1.2 NURBS

In general, B-splines are piecewise polynomials that offer great flexibility and precision for a myriad of modeling applications. They are built from a linear combination of basis functions that span a corresponding B-spline space [6, 7, 26]. These basis functions are locally supported and have continuity properties that follow directly from those of the basis [6]. However, there are geometric entities in $\mathbb{R}^{d_s}$ that cannot be modeled exactly by piecewise polynomials. Many important ones, however, can be obtained through a projective transformation of a corresponding B-spline entity in $\mathbb{R}^{d_s+1}$ yielding a rational B-spline. In particular, conic sections, such as circles and ellipses, can be exactly constructed by projective transformations of piecewise quadratic curves [4, 27, 28].

NURBS curve is a parametric curve, meaning that the points on the curve are swept out as the curve's parameter changes (Mathematically, the parameters of a curve or surface are the independent variables in the expression for the curve/surface). NURBS-based isogeometric analysis method can preserve the exact geometry, convenient for free-form surface modeling and also possesses special mathematical properties. NURNS basis functions can be refined through knot insertion; in fact each NURBS of order p is C^{p-1}- continuous. In addition convex hall and variation diminishing properties are other NURBS mathematical specifications [4, 27]. Consequently, these NURBS' merits properties have changed it to be interesting for fracture mechanics analysis. A NURBS surface and solid are defined as follows

$$\mathbf{S}(\boldsymbol{\xi}) = \sum_{\mathbf{i}\in I} \mathbf{P}_{\mathbf{i}}\, R_{\mathbf{i},\mathbf{p}}(\boldsymbol{\xi}), \qquad (1)$$

where $\mathbf{P}_i$ is a set of control points, $R_{\mathbf{i},\mathbf{p}}$ is multivariate basis function and ξ is a parameter value. A multivariate basis function is defined according to the univariate counterpart. Univariate B-spline basis functions for a given order p, are defined recursively in the parametric space by way

of the knot vector $\Xi = \{\xi_1, \xi_2, \xi_3, \ldots, \xi_{n+p+1}\}$. Where n is the number of basis functions which comprise the B-spline and are in a one to one correspondence with the control points and also are not in a one to one correspondence with the knots. A knot vector is a non-decreasing sequence of coordinates in the parametric space [29, 30]. The length of a knot vector is considered to $n+p+1$. The corresponding multivariate NURBS basis function is defined as [7]

$$R_{\mathbf{i},\mathbf{p}}(\boldsymbol{\xi}) = \frac{w_{\mathbf{i}} B_{\mathbf{i},\mathbf{p}}(\boldsymbol{\xi})}{\sum_{\mathbf{j}\in I} w_{\mathbf{j}} B_{\mathbf{j},\mathbf{p}}(\boldsymbol{\xi})}, \quad (2)$$

where $\{w_{\mathbf{i}}\}_{\mathbf{i}\in I}$, is a set of weights and I is the appropriate index set. A multivariate NURBS basis functions are defined using subsequent relation,

$$B_{\mathbf{i},\mathbf{p}}(\boldsymbol{\xi}) = \prod_{l=1}^{d_p} N^{l}_{il,pl}\left(\boldsymbol{\xi}^{l}\right), \quad (3)$$

where, $d_p = 1, 2, 3, \ldots$ is corresponding to the dimension of the problem and l must not confused with the power, hence this superscript implies any direction in the domain. Multivariate NURBS basis functions inherit most of the properties of their univariate counterparts, namely partition of unity, nonnegativity, compact support, higher-order continuity, and linear independence [7, 16].

Univariate B-spline basis functions $N_{i,p}$, is defined recursively using Cox-de-Boor formula as follows [29, 30]

First, beginning with piecewise constant ($p = 0$), then we have,

$$N_{i,0} = \begin{cases} 1 & \text{if } \xi_i \le \xi < \xi_{i+1}, \\ 0 & \text{Otherwise.} \end{cases} \quad (4)$$

So, for $p = 1, 2, 3, \ldots$ we define the basis functions according to the aforementioned formula, in this way

$$N_{i,p} = \frac{\xi - \xi_i}{\xi_{i+p} - \xi_i} N_{i,p-1}(\xi) + \frac{\xi_{i+p+1} - \xi}{\xi_{i+p+1} - \xi_{i+1}} N_{i+1,p-1}(\xi). \quad (5)$$

Figure 1 shows a NURBS surface and also some control points for instance which do not coincide the surface.

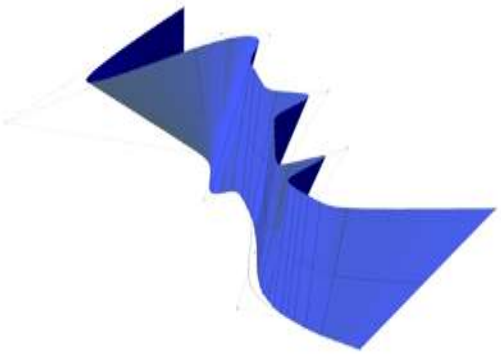

Figure 1: The NURBS Surface with its Associated Control Points.

1.3 T-splines

T-splines are introduced after point based splines, or simply PB-splines [31]. Researchers have been assumed PB-splines as a good alternative to the meshless methods. While smoothness is an important consideration, NURBS are severely limited by their tensor product construction. In traditional NURBS-based design, modeling a complicated engineering design often requires hundreds of tensor product NURBS patches which are usually discontinuous across patch boundaries [32, 33]. In addition, a NURBS surface is defined using a set of control points, which lie, topologically, in a rectangular grid. This means that a large number of NURBS control points may be superfluous in that they contain no significant geometric information, but merely are needed to satisfy the topological constraints [7, 26, 32, 34]. T-splines can model complicated designs as a single geometry. Unlike NURBS, T-splines can be locally refined. In other words, all local refinement is done on one control mesh and all control points have similar influence on the shape of the surface [35]. These properties make T-splines an ideal technology for isogeometric discretization and integrated design-through-analysis applications. Initial investigations using T-splines as a basis for isogeometric analysis demonstrated that the T-spline basis possesses similar convergence properties to NURBS with far fewer degrees-of-freedom [9, 26, 35-39]. Additionally, T-splines possess a natural finite element structure which can be integrated seamlessly into existing finite element frameworks via Bézier extraction [26, 33, 40]. T-splines have since been applied to problems in fracture and damage, and shells [19].

With NURBS, we used global knot vectors from which all the functions were defined. With PB-splines, each function had its own local knot vectors that remained completely independent of the other functions and their knot vectors. For T-

splines, a balance between the two cases has been performed. Each function will have its own local knot vector, but these local knot vectors be inferred from a global structure that encodes a topology and parameterization for the entire T-spline object. This global structure is called the T-mesh, and it is drawn in the index space of the T-spline. For more information on how a T-mesh is constructed see [35]. In fact, in the T-splines based isogeometric analysis, each basis function is calculated similar to the NURBS counterparts. But the major difference is in the knot vectors. Particularly, in the T-splines the local knot vectors are associated to each control points [31]. In this way, the scenes of local approach and the analysis that based on the element structure have been preserved.

A T-spline is defined in terms of a control grid (or, T-mesh) and global knot vectors $\vec{\mathbf{S}} = \left[s_{-1}, s_0, s_1, \ldots, s_{c+2}\right]$ and $\vec{\mathbf{t}} = \left[t_{-1}, t_0, t_1, \ldots, t_{r+2}\right]$. Each control point $\mathbf{T}_i$ corresponds to a unique pair of knots $\left(s_j, t_k\right)$, and will be referred to $\left(j, k\right)$ as the index coordinates of $\mathbf{T}_i$. A T-spline solid with its T-junctions in black circles is shown in Figure 2.

Figure 2: T-spline Solid with T-junctions at Upper Left Corner

$$\mathbf{T}\left(s,t\right) = \frac{\sum_{i=1}^{n_T} \mathbf{T}_i w_i T_i\left(s,t\right)}{\sum_{i=1}^{n_T} w_i T_i\left(s,t\right)}, \tag{6}$$

where $\mathbf{T}_i = \left(x_i, y_i, z_i\right) \in \mathbb{R}^3$ are control points, $w_i \in \mathbb{R}$ are weights, and n_T is the number of control points. $T_i\left(s,t\right)$ are blending functions, with

$$T_i\left(s,t\right) = B\left[\vec{\mathbf{s}}_i\right]\left(s\right) B\left[\vec{\mathbf{t}}_i\right]\left(t\right), \tag{7}$$

where $B\left[\vec{\mathbf{s}}_i\right]$ and $B\left[\vec{\mathbf{t}}_i\right]$ are blending functions in s and t directions respectively. These two different blending functions are calculated in a similar manner of NURBS basis functions, except their knot vectors are local and inferred from the T-mesh.

2. PRINCIPLES OF FRACTURE MECHANICS

In fact the behavior of a body with a discontinuity such as crack and flaw is generally characterized by a single parameter such as stress intensity factors (SIFs) in linear elastic fracture mechanics. Also, during last decades much effort has been done on SIFs calculation [41-47]. Theoretical, numerical and experimental methods have been employed for determination of the SIFs in the vicinity of crack tips in cracked bodies. There are three basic modes of deformation according to three independent kinematic movements of upper and lower crack surfaces with respect to each other. Any deformation of crack surfaces can be viewed as a superposition of these basic deformation modes, which are as opening, sliding and tearing (antiplane) modes. In 2D numerical analysis we only calculate the two first modes of deformations and so the corresponding stress intensity factors.

For two dimensional and any linear elastic body the crack-tip stress fields is given by a series of the form Eq. (8) which is known as Williams' asymptotic solution [48] as follows

$$\sigma_{ij}(r,\theta) = A_1 r^{-1/2} f_{ij}^{(1)}(\theta) + A_2 f_{ij}^{(\theta)} + A_3 r^{1/2} f_{ij}^{(3)}(\theta) + \text{higher order terms}, \tag{8}$$

where σ_{ij} is the stress tensor, r and θ are polar coordinates with the origin at the crack-tip. Also, $f_{ij}^{(1)}$, $f_{ij}^{(2)}$, $f_{ij}^{(3)}$ are universal functions of θ, and A_1, A_2, A_3 are parameters proportional to the remotely applied loads. In the vicinity of the crack tip, where ($r \to 0$), the leading term which has the denominator of square-root exhibits singularity. The amplitude of the singular stress fields is characterized by the stress intensity factors (SIFs), i.e. [49, 50]

$$\sigma_{ij} = \frac{K_{\mathrm{I}}}{\sqrt{2\pi r}} f_{ij}^{\mathrm{I}}(\theta) + \frac{K_{\mathrm{II}}}{\sqrt{2\pi r}} f_{ij}^{\mathrm{II}}(\theta), \tag{9}$$

where K_{I} and K_{II} are the mode I and mode II SIFs, respectively. By assuming the small-scale yielding in an elastic body, we can assume the crack as a semi-infinite domain. Hence, by ignoring the higher order terms in the series the first order

equations of the stress fields for mode I are as follows [50]

$$\begin{bmatrix}\sigma_{xx}\\ \sigma_{yy}\\ \tau_{xy}\end{bmatrix} = \frac{K_I}{\sqrt{2\pi r}}\cos\frac{\theta}{2}\begin{bmatrix}1-\sin\frac{\theta}{2}\sin\frac{3\theta}{2}\\ 1+\sin\frac{\theta}{2}\sin\frac{3\theta}{2}\\ \sin\frac{\theta}{2}\cos\frac{3\theta}{2}\end{bmatrix} \quad (10)$$

1.3 Cohesive zone formulation

Consider a solid $\Omega \subset \mathbb{R}^N \left(N = 2 \text{ or } 3\right)$ as depicted in Figure 3, the displacement of the material points $x \in \Omega$ is described by the displacement field $u \in \mathbb{R}^N$. The external boundary of the body is composed of a boundary Γ_u on which essential boundary conditions are provided, and a boundary Γ_t with natural boundary conditions. In addition and internal boundary Γ_d is present which represents either an adhesive interface between two separate regions, or a cohesive crack. Under the assumption of small displacements and displacement gradients, the deformation of the material is characterized by the infinitesimal strain tensor, $\varepsilon_{ij} = \frac{1}{2}\left(\frac{\partial u_i}{\partial x_j} + \frac{\partial u_j}{\partial x_i}\right)$. Furthermore, the crack opening $[\![u_i]\!]$ is defined as the difference between the displacements on either side of the internal discontinuity Γ_d. In the absence of body forces, the strong form quasi-static equilibrium equations are then given by

$$\begin{cases}\dfrac{\partial \sigma_{ij}}{\partial x_j} = 0 & x \in \Omega\\ u = \hat{u} & x \in \Gamma_u\\ \sigma_{ij} n_j = \hat{t}_i & x \in \Gamma_t\\ \sigma_{ij} n_j = t_i(u) & x \in \Gamma_d\end{cases} \quad (11)$$

However, the weak form of the equilibrium equations is obtained by multiplication with a virtual displacement δu and integration over the domain Ω. After the application of Gauss' theorem, this results in

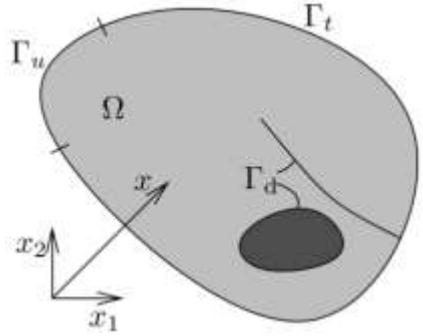

Figure 3: Representation of a Solid Body Ω with Internal Discontinuity Boundaries Γ_d.

$$\int_\Omega \sigma_{ij}\,\delta\varepsilon_{ij}\,d\Omega + \int_{\Gamma_d} t_i\,\delta\,u_i\;\;d\Gamma_d = \int_{\Gamma_t} \hat{t}_i\;\delta u_i\;d\Gamma_u\;, \quad (12)$$

where the prescribed boundary displacements and tractions are given by $\hat{u}$ and $\hat{t}$, respectively, and the Einstein summation convention has been used. From an implementation point of view, it is convenient to rewrite the weak form, Eq. (12), in the matrix-vector notation as

$$\int_\Omega \sigma^T\,\delta\gamma\,d\Omega + \int_{\Gamma_d} \mathbf{t}^T\,\delta\,u\;\;d\Gamma_d = \int_{\Gamma_t} \hat{\mathbf{t}}^T\;\delta\mathbf{u}\,d\Gamma_u\;, \quad (13)$$

where σ and γ are the Voigt form of the Cauchy stress tensor and engineering strain, respectively.

3. DISCONTINUOTIES IN B-SPLINES, NURBS AND T-SPLINES

The fundamental building block of isogeometric analysis is the univariate B-spline [4, 28, 51]. A univariate B-spline is a piecewise polynomial defined over a knot vector $\Xi = \{\xi_1,\ \xi_2, \xi_3, \ldots, \xi_{n+p+1}\}$. Where n is the number of basis functions and p is the polynomial order. As a consequence, the knots divide the parametric domain $\left[\xi_1, \xi_{n+p+1}\right] \subset \mathbb{R}$ in knot intervals of non-negative length. We refer to knot intervals of positive length as elements, so, we have the knot elements. When several knot values coincide, their multiplicity is indicated by m_i, where i corresponds to the index of the knot values. The B-splines used for analysis purposes are generally open B-splines, which means that the multiplicity of the first and last knots (i.e. m_1 and m_{n+p+1}) are equal to $p+1$. The property of NURBS of particular interest for fracture mechanics is that they are $p - m_i$ times

continuously differentiable over a knot i. This allows for the direct discretization of higher-order differential equations [52]. The ability to control inter-element continuity is useful for cohesive zone models, since discontinuities can be inserted arbitrarily by means of knot insertion. In fact, a jump in the displacement field at a certain point $x_d = x(\xi_d)$ in the physical space can be created by raising the multiplicity of the knot ξ_d to $m_i = p+1$.

To demonstrate the inter-element (i.e. knot element) continuity control in NURBS basis functions we create a 3D model with the number of 715 control points in a topologically rectangular arrangement. In this model we assumed the polynomial orders in *x*, *y* and *z* directions as 3, 3 and 2, respectively. In this situation if we consider the multiplicity of a knot value as 3 in *x* or *y* directions and 2 in *z* direction, we will have a C^0 continuity. In other words, this procedure discretizes our interest domain into a finite element mesh with the C^0 inter element continuity at its corresponding knot value. However, in a NURBS solid which the parameter fields and the geometry is approximated using the same basis functions, we can see a jump line as C^0 line. Figure 4 illustrates the C^0 continuity line at the knot value of 0.5 in *x* and *y* directions of the 5×7×4 domain. The material behavior is assumed as linear elastic and loading condition is uniaxial tension in *y* direction.

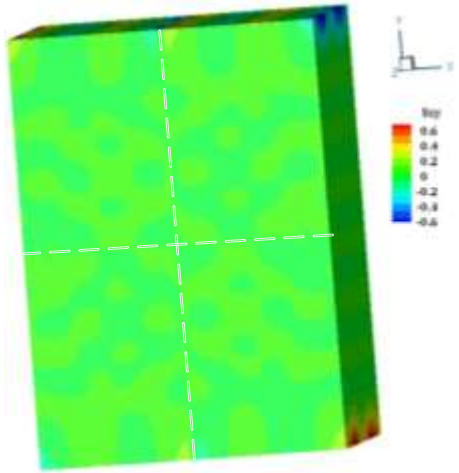

Figure 4: Stress Distribution for a 3D NURBS Model with C^0 Continuity at half of the width and height.

However, we can create a global discontinuity in throughout a domain by using aforementioned property of B-splines basis functions. As it shown in Figure 5, we can create a throughout discontinuous basis functions using knot vectors in parametric space. In fact if there is a knot value in the knot vector which has the multiplicity equal to $p+1$, then the influences of a global cohesive discontinuity occurs in the physical space. In this example a rectangular domain with a global discontinuity which cut the domain into two separate parts is studied to introduce the global vision of cohesive zone generating using NURBS-based isogeometric analysis. In fact, the special features of continuity control in NURBS basis functions simplify this object. In the following example we create the desire domain of 5×7 plate with one patch by using these knot vectors in two directions. $\Xi = \{0, 0, 0, 0, 1/3, 2/3, 1, 1, 1, 1\}$, $H = \{0, 0, 0, 0, 1/3, 1/3, 1/3, 1/3, 1, 1, 1, 1\}$. This domain is created using polynomial order 3 in both *x* and *y* geometrical directions. So, by utilizing the open knot vectors, the multiplicities of the first and last knots are 4. Also, in this case by inserting a knot at $\eta = \eta_d = 1/3$ in the knot vector H with multiplicity one more than the associated polynomial order a discontinuity is created. The result is shown in Figure 6.

It should be noted that in the case of the small deformation cohesive zone formulation, the continuity of position vector is preserved by constraining the control point positions and their weights on either side of the discontinuity. In this study to fulfill the continuity those constraints are imposed by equating the positions and weights of the control points on the crack surfaces.

The material behavior is assumed as linear elastic and the loading condition is considered as uniaxial tension. Accordingly, by using parametric space capabilities in isogeometric analysis, the studying of a pre-cracked domain is easy to reach.

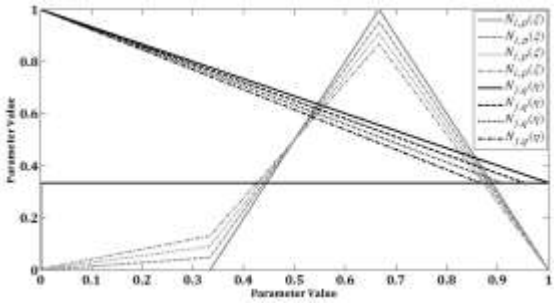

Figure 5: Discontinuous NURBS Basis Functions

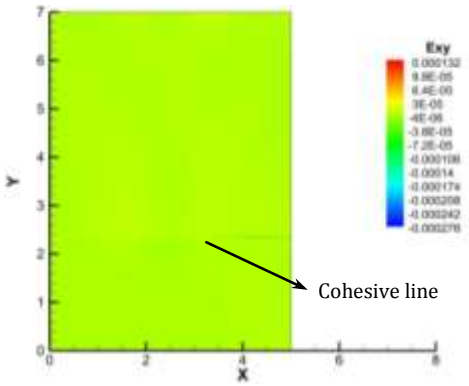

Figure 6: A Jump in Strain Distribution in a Single Patch at The Parametric Value of $\eta = 1/3$.

In this contribution a 3D model is created to show the effects of cohesive zone modeling in a NURBS body. In this example we utilized polynomials of order 3 in both *x* and *y* directions and a polynomial order 2 in *z* direction. This NURBS solid body is comprised of one patch with the size of 5×7×4. The length of knot vectors in *x*, *y* and *z* directions are 15, 17 and 8 respectively. The constitutive of material is considered as linear elastic. The loading condition is uniaxial tension, $\sigma = 1(\text{MPa})$, which is applied on both sides of the body in *y* direction. Figure 7 depicts NURBS' control mesh for the solid body with a cohesive surface at parametric value of, $\eta = 1/3$.

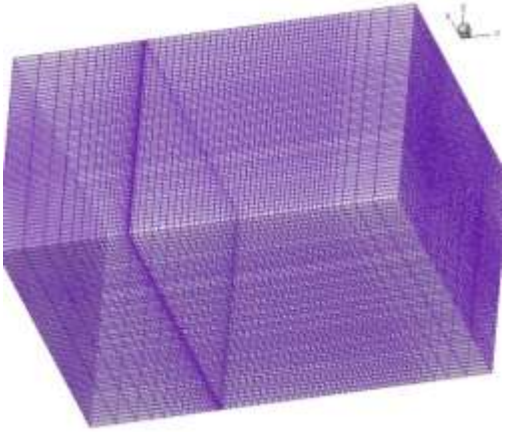

Figure 7: 3D NURBS Solid with its Control points mesh.

Figure 8 demonstrates the jump in the ε_{yy} in the presence of a cohesive surface in NURBS solid. In fact a jump in strain results is obvious; as a consequence a global discontinuous surface is created without any manipulation in physical space.

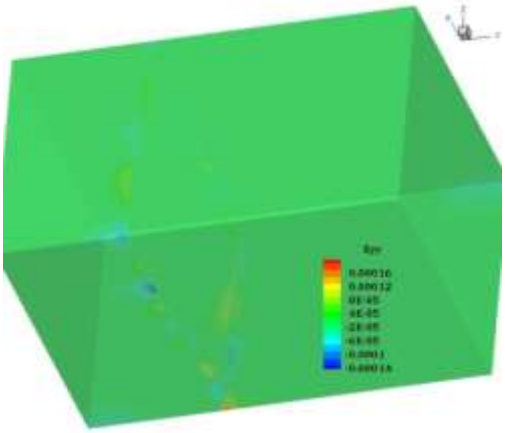

Figure 8: 3D NURBS Solid with a Cohesive Zone at 1/3 of its height.

Also we create a discontinuity in a domain with the repetition of different control points between two patches. Due to this procedure a singularity occurs in the stiffness matrix and we can capture the effects of a strong discontinuity in the physical space. In Figure 9 and Figure 10 we illustrate different methods for creation discontinuities in the isogeometric analysis framework. We utilize this procedure to analysis a domain with local strong crack discontinuity such as edge and center cracks.

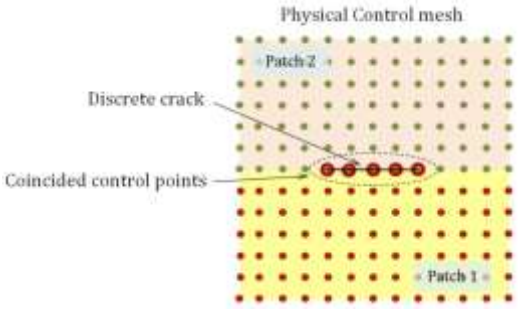

Figure 9: Creating the Strong Discontinuity Using Physical Control Points.

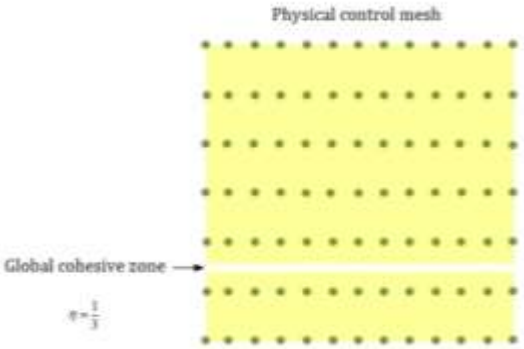

Figure 10: Creating Cohesive zone using knot vector.

4. DISCRETIZATION OF SOLIDS USING NURBS

In this section to summarize the contents of the paper only the formulation of two dimensional problems is discussed. NURBS (or B-spline), basis functions are used for both the parameterization of the geometry and the approximation of the solution space for the displacement field **u** that is

$$\mathbf{u}(\xi,\eta)=\sum_{i=1}^{n}\sum_{j=1}^{m}R_{i,j}^{p,q}(\xi,\eta)\mathbf{U}_{i,j}, \quad (14)$$

where $R_{i,j}^{p,q}$ are the bivariate NURBS basis functions and $\mathbf{U}_{i,j}$ are the displacement control variables.

The parameterization of a body $\Omega \subset \mathbb{R}^2$ can be obtained by a NURBS surface. Such a surface can be comprised of one or more NURBS surfaces. A two-dimensional NURBS patch (i.e. any B-spline associated with a particular set of knot vectors, polynomial orders and control points is referred as a patch.) gives a bivariate parameterization of Ω based on the knot vectors

$\Xi=\{\xi_1,\ \xi_2,\ \xi_3,...,\xi_{n+p+1}\}$, and,

$\mathrm{H}=\{\eta_1,\ \eta_2,\ \eta_3,...,\eta_{m+q+1}\}$, such that

$(\xi,\ \eta)\in[\xi_1,\ \xi_{n+p+1}]\otimes[\eta_1,\ \eta_{m+q+1}]\subset\mathbb{R}^2$.

$$\mathbf{x}(\xi,\eta)=\sum_{i=1}^{n}\sum_{j=1}^{m}R_{i,j}^{p,q}(\xi,\eta)\mathbf{X}_{i,j}, \quad (15)$$

where $\mathbf{X}_{i,j}$ are the coordinates of the control points. It should be noted that when all weights of control points are equal and in the especial form equal to one, so, NURBS basis functions degenerate to B-spline counterparts. The bivariate and trivariate NURBS basis functions are given by

$$R_{i,j}^{p,q}(\xi,\eta)=\frac{N_{i,p}(\xi)M_{j,q}(\eta)W_{i,j}}{\sum_{i=1}^{n}\sum_{j=1}^{m}N_{i,p}(\xi)M_{j,q}(\eta)W_{i,j}}, \quad (16)$$

$$R_{i,j,k}^{p,q,r}(\xi,\eta,\zeta)=\frac{N_{i,p}(\xi)M_{j,q}(\eta)L_{k,r}(\zeta)W_{i,j,k}}{\sum_{i=1}^{n}\sum_{j=1}^{m}\sum_{k=1}^{s}N_{i,p}(\xi)M_{j,q}(\eta)L_{k,r}(\zeta)W_{i,j,k}}. \quad (17)$$

where $N_{i,p}(\xi)$, $M_{j,q}(\eta)$ and $L_{k,r}(\zeta)$ are univariate B-spline basis functions defined over knot vectors Ξ, H, Z respectively. The set of control points and associated weights named as control net.

5. NUMERICAL EXAMPLES USING NURBS-BASED IGA

In this section NURBS surfaces with predefined strong discontinuity such as edge and center cracks are considered. First of all, for each plate which assumed under uniaxial tension, the comparison between the exact solution and the isogeometric analysis results are performed to show the accuracy of the numerical solutions. All NURBS surfaces are created with polynomial order 3 in both geometrical directions. The stress distribution condition is assumed as plane strain and the material constitutive is considered as linear elastic. In addition the solid NURBS with predefined strong discontinuity are generated. Eventually, the values of the stress intensity factors are numerically calculated and also compared with the analytical-experimental counterparts.

1.3 Edge crack example

In the first example a predefined edge crack with the length of 0.5 in a 3×6 plate under uniaxial tension is modeled. This domain is comprised of 1233 control points. As a matter of fact the arrangement of control points is considered in a manner to have the maximum control on the NURBS surface in the vicinity of the crack tip. So, we have the topologically rectangular finer control net around the crack tip. In addition, to increase the precision of the numerical integration we have used the finer parametric space in the vicinity of the crack tip. Therefore, we have the finer knot spans around the crack tip. Also, due to capturing the sudden changes in stresses at the crack tip, the polynomial order 3 are utilized in all geometrical directions. This example is constructed with two patches, and every patch contains 625 individual control points. Hereupon, the length of each knot vector must be considered as 29 distinct knot values. All knot vectors are open, so, the first and last knot values multiplicities are 4. The constitutive of material is assumed as linear elastic with the properties of $E=1.0E6(\mathrm{MPa})$ and $\nu=0.3$. Figure 11 illustrates the stress distribution and stress concentration at the crack tip and also Figure 12 depicts the smooth sudden changes that occur in the plate with an edge crack.

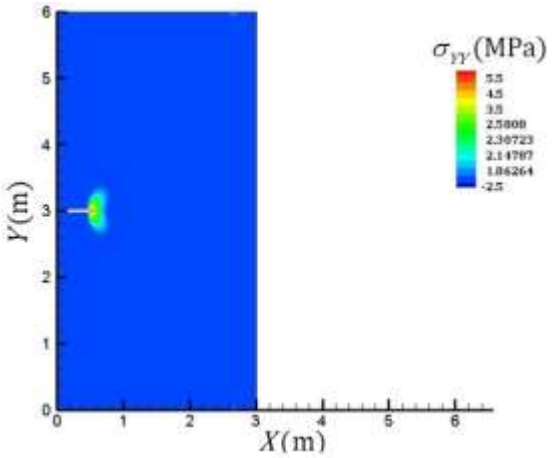

Figure 11: σ_{yy} Distribution in an Edge Cracked Plate

What is so crucial in computational fracture mechanics using isogeometric analysis is the smoothness of stress distribution throughout the body, particularly in the vicinity of the crack tips. It should be noted that, the precision of stress and strain at the crack tips are very important, since they are used to calculate the stress intensity factors. Unlike other numerical approaches the inter-element degrees of continuity is easily obtained in the isogeometric analysis framework. Hence, a comparative calculation is performed to demonstrate the condition of the numerical results. Figure 13 shows the conformation of the numerical results to the analytical-experimental solution for the stress fields.

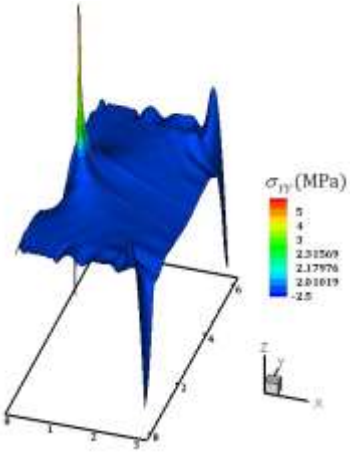

Figure 12: Smooth Sudden Changes in Stress Distribution.

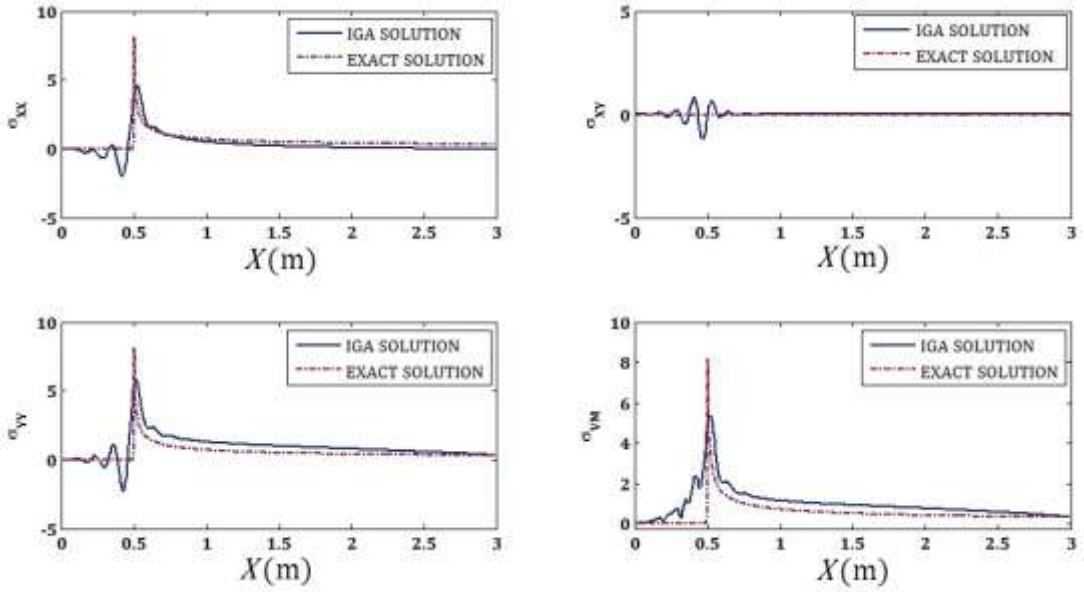

Figure 13: Comparison between the IGA Edge Crack Model and the Exact Solution.

In this example a 3D model is generated to show the effects of a discontinuous edge surface in the solid NURBS. The interest domain is created by using 6170 global control points. The arrangement of the control points is chosen in a manner to have the maximum control on the geometry conditions at the crack surfaces. Hence, the differences between consequent control points decreased gradually till the crack surfaces. This three dimensional solid NURBS is comprised of two patches. In all patches the polynomial orders in *x* and *y* directions are assumed 3 and in the *z* direction is considered 2. The loading condition is considered as uniaxial tension which applies in *y* direction. Figure 14 and Figure 15 illustrate the stress distribution and concentration in two different patches. In order to visualize the discretization of the NURBS volume the physical control mesh is shown.

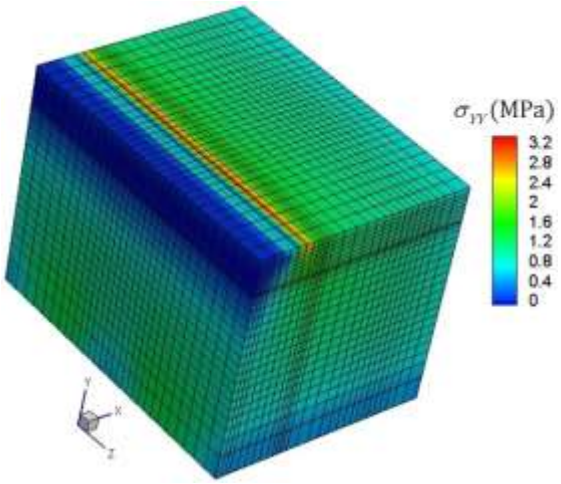

Figure 14: Three Dimensional NURBS Volume with Predefined Edge Crack, (First Patch).

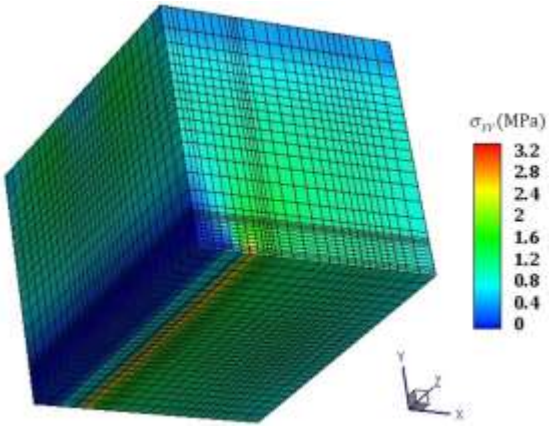

Figure 15: Three Dimensional NURBS Volume with Predefined Edge Crack, (Second Patch).

2.3 Center crack example

In the following example a predefined center crack with the length of 0.5 in a 3×6 plate under uniaxial tension is modeled. In order to visualize the effects of the control point's pattern, this domain are discretized by using of the 1230 and 4010 physical control points. As a matter of fact the arrangement of control points is considered in a manner to have the maximum control on the NURBS surface in the vicinity of the crack tips. So, we have the topologically rectangular finer control net around the crack tips. In addition, to increase the precision of the numerical integration we have used the finer parametric space in the vicinity of the crack tips. Therefore, we have the finer knot spans around the crack tips which are assumed symmetric for both crack tips. Also, due to capturing the sudden changes in the stresses at the crack tips, the polynomial order 3 are utilized in all geometrical directions for 2D example. This example is constructed with two patches, and in two different discretizing schemes, every patch contains 625 or 2025 individual control points, respectively. The arrangements of the control points in two models were chosen 25×25 and 45×45 for each patch. Hereupon, the length of the each associated knot vector must be considered as 29 and 49 distinct knot values for both models, respectively. All knot vectors are open, so, the first and last knot values multiplicities are 4. The constitutive of material for stress distribution condition is plane strain and the properties of elasticity are assumed $E = 1.0\,\mathrm{E}^6$ (MPa) and $\nu = 0.3$. Figure 16 and Figure 17 illustrates the stress distribution and stress concentration at the crack tips and also the sudden changes that occurs in the plate.

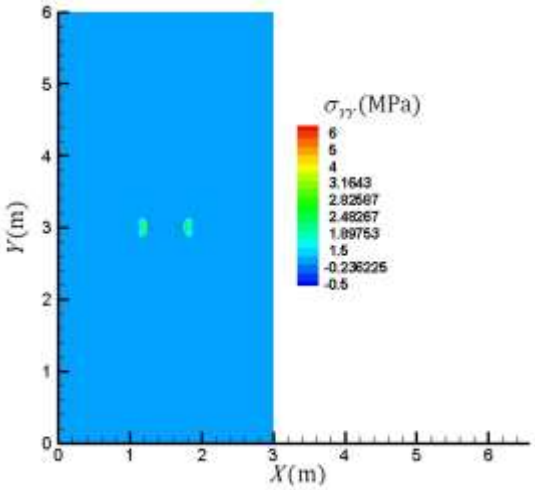

Figure 16: Isogeometric analysis result of σ_{yy} distribution for center crack example.

June. 2015. Vol. 7. No. 01 ISSN2305-8269
International Journal of Engineering and Applied Sciences

www.eaas-journal.org

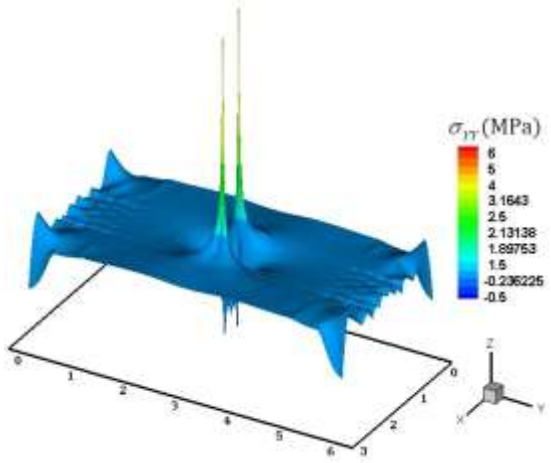

Figure 17: Exact Stress Concentration Modeling at the Crack Tips.

Then, in order to demonstrate the smoothness of the stress distribution in throughout the plate, we extract the obtained results at the level of the crack (i.e. $y = 3$) and finally compare them with the exact solutions. Numerical results represent a significant adaptation with the exact counterpart amounts. In fact utilizing polynomial order three preserve the smoothness and precision of the stresses and strains. Figure 18 represents the conformation of the exact and IGA results for the plate with one center crack.

As we know one of the most important issues in the numerical approaches is the stiffness matrix. However, in this example with two different degrees of freedom (DOFs) we have two stiffness matrices with their particular own properties. Among various properties of the stiffness matrix, we restrict ourselves to the "stiff index" which is defined as the maximum to minimum ratio of the corresponding Eigen values. In the domain with 2460 degrees of freedom the stiff index was equal to 1.85 and also in the domain with 8020 degrees of freedom the stiff index was 1.69. This means that in the second condition with more DOFs the differences of the corresponding Eigen values are less than the first condition with less DOFs. In other words the effects of singularity in the stiffness matrix would become better with the finer discretization at the crack tips. The finer discretization not only is obtained by using finer physical control mesh but also in the parametric space. However, more DOFs improve the stiffness matrix condition.

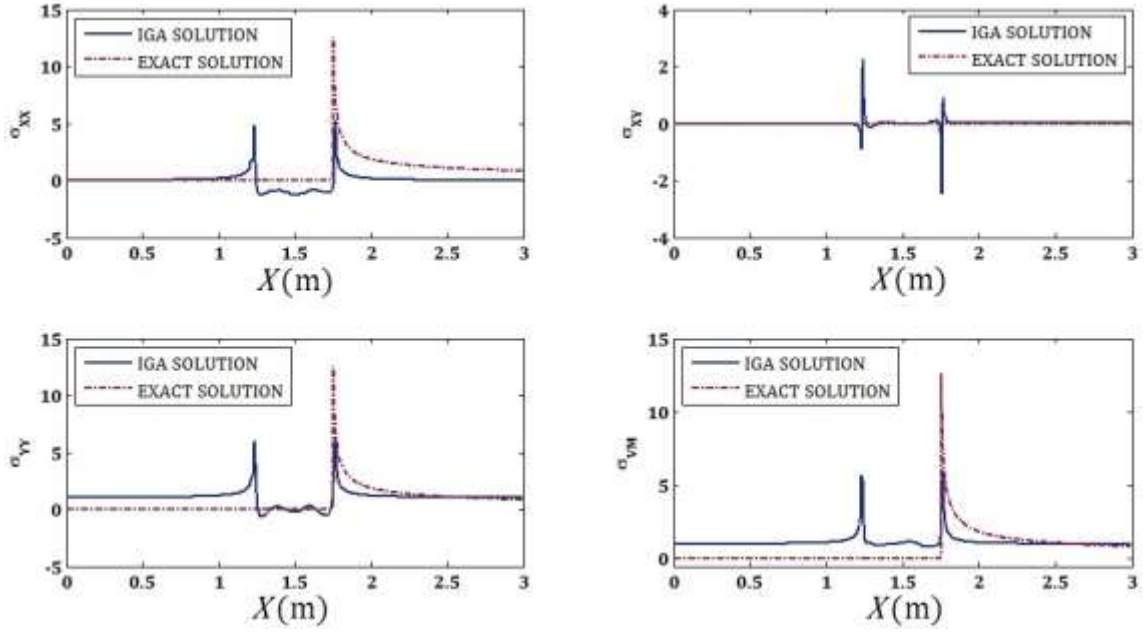

Figure 18: Representation of the Isogeometric Analysis Results and Exact Solution.

In addition this example is analyzed in three dimensional situation. In the case of 3D center discontinuous surface we utilized two patches. The degrees of approximant polynomials are considered as 3, 3 and 2 in geometrical directions of x, y and z, respectively. The present 3D NURBS volume is consist of 6150 physical control points in a coordinates in which we have a finer mesh near the crack tip surfaces. Figure 19 shows the three dimensional NURBS volume with a center crack

which is generated by using the repetition of adjacent control points in two patches. In fact in this 3D volume that created exactly via NURBS basis functions we considered the influences of a discontinuous surface much easier than other numerical approaches with no excess mathematical computations. However, the simplifications which isogeometric analysis method is induced in the fracture mechanics are introduced. Eventually, we can calculate the main parameter of the linear elastic fracture mechanics such as stress intensity factors easily and preciously.

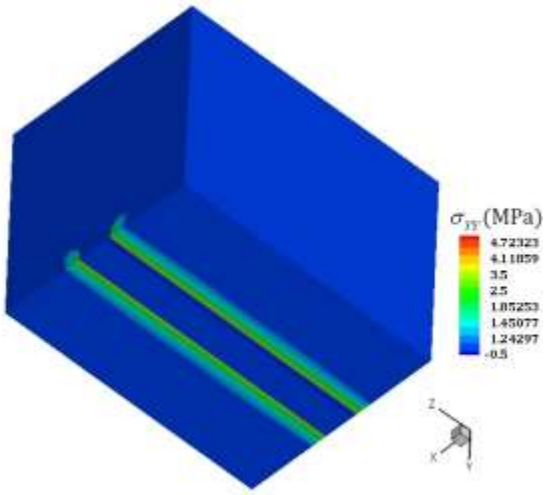

Figure 19: Three Dimensional NURBS Volume with a Predefined Center Crack.

3.3 Stress intensity factors calculation

Facture behavior is generally characterized by using a single parameter such as stress intensity factor. There are analytical and experimental solutions for some simple and idealized domain with specific boundary conditions. So, in order to describe the behavior of a cracked body we have to use the numerical methods to calculate fracture parameters. For more information about analytical-experimental solutions see [50, 53, 54]. According to the analytical-experimental solution for edge crack, the stress intensity factor of mode I introduced as Eq. (18) [50, 53, 54]. In this work we attempt to demonstrate the possibility of isogeometric analysis method in calculating of the fracture mechanic parameters. So, the values of computational stress intensity factors for mode one and two are compared with the analytical-experimental counterparts. Therefore, in the plane strain condition and for a plate with the width of 3 and the height of 6 the values of SIFs are calculated using stress extrapolation method. This procedure is conducted for the problems of edge crack and center crack. In this comparison the length of each kind of the crack is chosen variable. In fact, according to the geometry restrictions, the lengths of the crack (i.e. edge or center) are varied from 0.1 to 2.0. In the case of the edge crack problems the amounts of the analytical-experimental SIFs are calculated using Eq. (18).

$$K_I = \left[1.12 - 0.23\left(\frac{a}{b}\right) + 10.56\left(\frac{a}{b}\right)^2 - 21.74\left(\frac{a}{b}\right)^3 + 30.42\left(\frac{a}{b}\right)^4 \right] \sigma\sqrt{\pi a} \qquad (18)$$

where a is the crack length and b is the width of the domain.

Table ***1*** and Figure 20 illustrate the compatibility of the computational and the analytical SIFs which are calculated for a plate with an edge crack. Because the width of the domain is 3, so, when the edge crack length is 2.0, and as it approaches to the boundary of the domain, we have the maximum error in SIFs.

The same procedure is performed to calculate the SIFs for the center crack. The horizontal center cracks with different lengths are modeled to examine the capability of the method in fracture mechanics. In fact, having the precise mixed mode stress intensity factors will help us to understand the accurate crack initiation angle growth. All present examples are under uniaxial tension loading. According to the geometry configuration and loading conditions we obtained symmetric results for both crack tips in the domain. Results are listed in Table 2, as it shown the error slightly increase in estimating the SIFs as the length of the center crack increases. While the crack tips are approaching to the edges of the domain (i.e. geometrical boundaries), hence, the error increased. To fulfilling the comparison of the values of numerical and analytical-experimental SIFs, the values of the SIFs for center cracks are calculated using Eq. (19).

$$K_I = \left[1 + 0.256\left(\frac{a}{b}\right) - 1.152\left(\frac{a}{b}\right)^2 + 12.2\left(\frac{a}{b}\right)^3 \right] \sigma\sqrt{\pi a} \qquad (19)$$

Also, Figure 21 illustrates the compatibility of the numerical and analytical-experimental values of SIFs for center crack problems.

Table 1: Comparison between Analytical-Experimental Values of Stress Intensity Factors and Numerical Results for Edge Crack Problems

Crack length	Analytical-Experimental K_I	Numerical K_I	Numerical K_{II}	K_I(Numerical)/K_I(Analytical)
0.1	0.6296	0.6251	0.0018	0.993
0.2	0.9082	0.9135	0.0025	1.006
0.3	1.1493	1.1547	0.0032	1.005
0.4	1.3846	1.3869	0.0038	1.001
0.5	1.6266	1.6258	0.0044	0.999
0.6	1.8825	1.8789	0.0051	0.998
0.7	2.1581	2.1535	0.0058	0.998
0.8	2.4591	2.4532	0.0008	0.998
0.9	2.7927	2.7905	0.0009	0.999
1.0	3.1674	3.1708	0.001	1.001
1.5	6.1407	6.1340	0.0161	0.999
2.0	13.1032	13.4695	0.0038	1.028

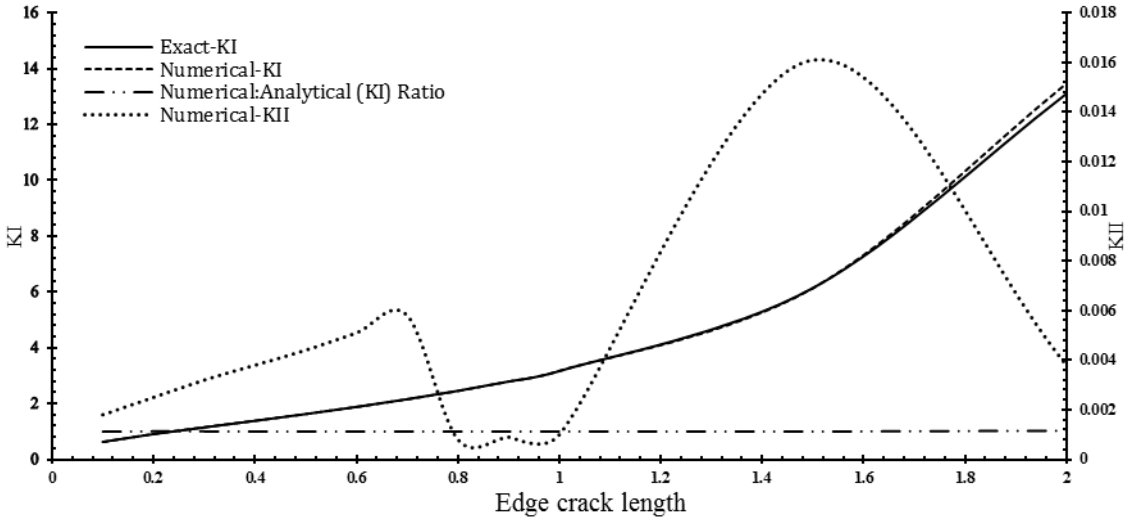

Figure 20: Consistent Numerical and Theoretical Calculations of the SIFs for Edge Crack problems.

Table 2: Comparison between Analytical-Experimental Values of Stress Intensity Factors and Numerical Results for Center Crack Problems

Crack length	Analytical-Experimental K_I	Numerical K_I	Numerical K_{II}	K_I(Numerical)/K_I(Analytical)
0.1	0.3979	0.3982	0.0000	1.001
0.2	0.5648	0.5434	0.0000	1.01
0.3	0.6943	0.6787	0.0000	0.976
0.4	0.8050	0.7919	0.0000	0.984
0.5	0.9043	0.8988	0.0000	0.994
0.6	0.9963	0.9810	0.0000	0.985
0.7	1.0838	1.0701	0.0000	0.987
0.8	1.1687	1.1566	0.0000	0.990
0.9	1.2528	1.2422	0.0000	0.992
1.0	1.3375	1.3278	0.0000	0.993
1.5	1.8153	1.7940	0.0000	0.988
2.0	2.4977	2.4517	0.0000	0.982

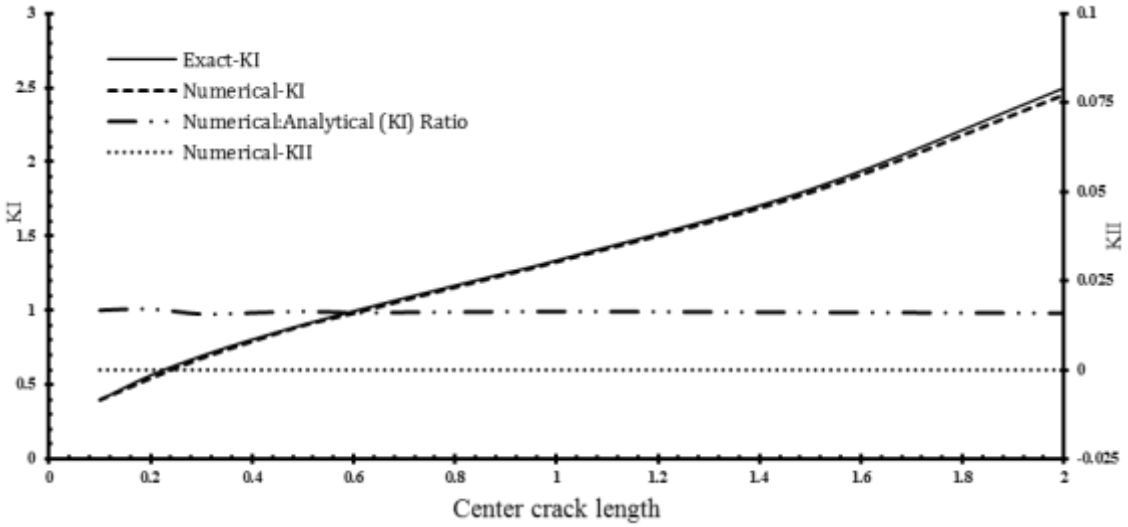

Figure 21: Adjacent Between Numerical and Theoretical Calculation of the SIFs.

Consequently, we can calculate the accurate crack initiation angle based on the maximum Hoop stress criterion for mixed mode of crack propagation. In fact, the exact crack propagation angle inferred from the precise stress intensity factors. In the previous examples for edge and center cracks the initiation angle of crack growth is zero due to the fact that the loading condition is uniaxial tension and the cracks are considered horizontal, therefore, there are mode one predominant.

6. DISCRETIZATION OF A SOLID WITH T-SPLINES

Because of some limitations which associated with NURBS technology, it is therefore attractive to use T-splines. In general, the localized basis function inference is the major motivation behind a T-spline. In this section we briefly discussed about local approach in T-spline-based isogeometric analysis. The basis functions, $R_{i,j}^{p,q}$, completely defined by a set of local knot vectors $\Xi_{i,j} \subset \Xi$ and $\mathrm{H}_{i,j} \subset \mathrm{H}$ of length $p+2$ and $t+2$, respectively. Where p and t are assumed polynomial orders. In the case that the orders p and t are odd, to which we will restrict ourselves in this work, the knot vectors associated with the vertex (i, j) in the index space are

$$\Xi_{i,j} = \left\{ \xi_{i-\frac{p+1}{2}}, \ldots, \xi_i, \xi_{i+\frac{p+1}{2}} \right\} \quad \text{and}$$

$$\mathrm{H}_{i,j} = \left\{ \eta_{i-\frac{q+1}{2}}, \ldots, \eta_i, \eta_{i+\frac{q+1}{2}} \right\}.$$

Therefore, we can calculate the associated T-spline basis functions respect to those local knot vectors in the subsequent relations. Consider (s, t) as the local coordinates of Gauss point. So, a numerical subroutine in the computer program returns the values of all basis functions evaluated at the Gauss point as well as the values of the derivatives of all basis functions with respect to s and t evaluated at Gauss point. This subroutine computes the value of the ith basis function and its derivatives, where i ranges from one to number of nodes in the domain. Eq. (20) describes the derivatives of T-spline basis functions. It must be taken into account that the T-spline basis functions are numerically calculated the same as the NURBS counterparts.

$$\frac{\partial N^{(i)}}{\partial s}(s,t) = \frac{W^{(i)} \frac{dS^{(i)}}{ds}(s) T^{(i)}(t) - N^{(i)}(s,t) \sum_{j=1}^{\text{nnode}} W^{(j)} \frac{dS}{ds}(s) T^{(j)}(t)}{\sum_{j=1}^{\text{nnode}} W^{(j)} S^{(j)}(s) T^{(j)}(t)} \tag{20}$$

where the values of $\frac{dS^{(i)}}{ds}(s)$ and $\frac{dT^{(i)}}{dt}(t)$ are calculated by sending the s-coordinate of the Gauss point to the subroutine which is corresponding to the T-spline basis functions calculation.

In this contribution a test example using T-spline is presented. In this example a plate with a hole is created and the stresses are obtained. The plate is an infinite plate with circular hole under constant in-plane tension. Specifically, the plate is subjected to tensile stress σ_t; the radius of the circular hole α is equal to 5 in; the width of the plate is equal to 40

inches; the thickness of the plate is equal to 0.1 inch; the Poisson's ratio ν is equal to 0.3 and the Young's modulus E equals 6.89E+04 (MPa). For simplicity and analysis reasons, the infinite plate is reduced to a finite quarter plate.

Since a T-spline based isogeometric analysis needs to a T-mesh to infer the local knot vectors for every anchor (namely, the control points), the associated T-mesh for aforementioned example is illustrated in Figure 22. The corresponding T-mesh in the parametric space contains no rectangular topology. Particularly the anchors or control points are not in a rectangular arrangement.

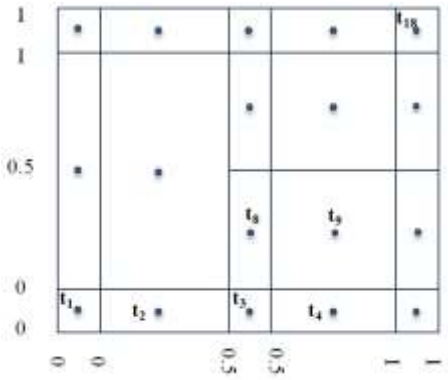

Figure 22: T-Mesh for Plate with a Hole in the Parametric Space. Control Points are shown in Blue Solid Circles.

Accordingly, the associated basis functions for each control points are calculated via each pair of local knot vectors. To alleviate the excessive context in this paper we briefly describe a specimen for inference of a pair of local knot vectors. Consider control point $\mathbf{t}_8$, then the horizontal and vertical local knot vectors are as follows

$$\begin{aligned} \Xi_{\mathbf{t}_8}^{(\text{Horizontal})} &= \{0, 0, 0, 0.5\}, \\ \mathrm{H}_{\mathbf{t}_8}^{(\text{Vertical})} &= \{0, 0, 0, 1.0\}. \end{aligned} \tag{21}$$

It should be noted that these knot vectors are for two quadratic polynomials in two directions, therefore, the length of these knot vectors are 4 (i.e. they contain 4 different knot values). In the present example test, the weight values for the control points $\mathbf{t}_2, \mathbf{t}_3, \mathbf{t}_4$ is equal to 0.85355 and it means that they are in the 62.80°, also the weight of $\mathbf{t}_8, \mathbf{t}_9$ is equal to 0.92678 which means that they are located at 44.12° with respect to the origin in the lower right corner. The weight is calculated by using a relation respected to the rational Bezier curve generation [4]. Figure 23 shows the stress distribution in the plate with a quarter holes.

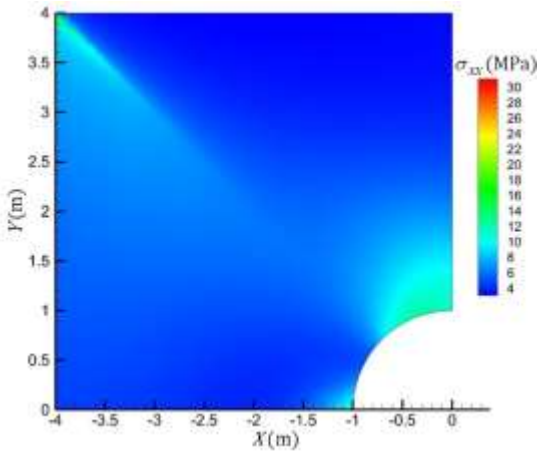

Figure 23: Stress Distribution and Concentration in the Plate with a Quarter Hole.

7. CONCLUSION

In this contribution we utilized two different computational geometry technologies in the structural analysis and also fracture mechanics. NURBS with global and T-splines with local knot vectors are utilized in engineering analysis problems. T-splines reduce the degrees of freedom in analysis and hence reduce the computational efforts. The possibility of enhancing a B-spline with knot insertion in the parametric space performed preciously to create cohesive zones and strong discontinuity in the physical space without excessive manipulating of the physical domain. Also, geometries are generated exactly by using NURBS-based isogeometric analysis method. In fact expressions of well-known h, p and hp refinement in FEM are implemented in the concept of isogeometric analysis to obtain the best results. The comparisons between analytical-experimental and numerical results for stress intensity factors demonstrate the applicability of the isogeometric analysis method in the context of fracture mechanics and crack propagation problems. In addition we used different types of polynomial orders in one NURBS solid. Finally, T-splines with the property of local refinement could decrease superfluous control points.

REFRENCES

[1] Z. Zhuang, Z. Liu, B. Cheng, J. Liao, "Chapter 2 - fundamental linear elastic fracture mechanics", In: Zhuang Z, Liu Z, Cheng B, Liao J, editors. Extended finite element method. Oxford: Academic Press, 2014, pp. 13-31.

[2] S.D. Daxini, J.M. Prajapati, "A review on recent contribution of meshfree methods to structure and fracture mechanics applications", *The Scientific World Journal*, Vol., No., 2014, pp.

[3] T. Chen, Z.-G. Xiao, X.-L. Zhao, X.-L. Gu, "A boundary element analysis of fatigue crack growth for welded connections under bending", *Engineering Fracture Mechanics*, Vol. 98, 2013, pp. 44-51.

[4] T.J.R. Hughes, J.A. Cottrell, Y. Bazilevs, "Isogeometric analysis toward integration of cad and fem", 2009, p. 355.

[5] J.A. Cottrell, T.J.R. Hughes, Y. Bazilevs, "Isogeometric analysis: Toward integration of CAD and FEA", Wiley, 2009.

[6] T.J.R. Hughes, J.A. Cottrell, Y. Bazilevs, "Isogeometric analysis: Cad, finite elements, NURBS, exact geometry and mesh refinement", *Computer Methods in Applied Mechanics and Engineering*, Vol. 194, No. 39–41, 2005, pp. 4135-4195.

[7] Y. Bazilevs, V.M. Calo, J.A. Cottrell, J.A. Evans, T.J.R. Hughes, S. Lipton, et al., "Isogeometric analysis using T-splines", *Computer Methods in Applied Mechanics and Engineering*, Vol. 199, No. 5–8, 2010, pp. 229-263.

[8] M.-J. Choi, S. Cho, "Isogeometric shape design sensitivity analysis of stress intensity factors for curved crack problems", *Computer Methods in Applied Mechanics and Engineering*, Vol. 279, 2014, pp. 469-496.

[9] J. Li. Isogeometric finite element analysis using T-splines: Brigham Young University. Department of Civil and Environmental Engineering; 2009.

[10] J.A. Evans, Y. Bazilevs, I. Babuška, T.J.R. Hughes, "N-widths, sup–infs, and optimality ratios for the k-version of the isogeometric finite element method", *Computer Methods in Applied Mechanics and Engineering*, Vol. 198, No. 21–26, 2009, pp. 1726-1741.

[11] J.A. Cottrell, T.J.R. Hughes, A. Reali, "Studies of refinement and continuity in isogeometric structural analysis", *Computer Methods in Applied Mechanics and Engineering*, Vol. 196, No. 41–44, 2007, pp. 4160-4183.

[12] J.A. Cottrell, A. Reali, Y. Bazilevs, T.J.R. Hughes, "Isogeometric analysis of structural vibrations", *Computer Methods in Applied Mechanics and Engineering*, Vol. 195, No. 41–43, 2006, pp. 5257-5296.

[13] I. Akkerman, Y. Bazilevs, C.E. Kees, M.W. Farthing, "Isogeometric analysis of free-surface flow", *Journal of Computational Physics*, Vol. 230, No. 11, 2011, pp. 4137-4152.

[14] Y. Bazilevs, I. Akkerman, "Large eddy simulation of turbulent taylor–couette flow using isogeometric analysis and the residual-based variational multiscale method", *Journal of Computational Physics*, Vol. 229, No. 9, 2010, pp. 3402-3414.

[15] Y. Bazilevs, V.M. Calo, J.A. Cottrell, T.J.R. Hughes, A. Reali, G. Scovazzi, "Variational multiscale residual-based turbulence modeling for large eddy simulation of incompressible flows", *Computer Methods in Applied Mechanics and Engineering*, Vol. 197, No. 1–4, 2007, pp. 173-201.

[16] Y. Bazilevs, M.C. Hsu, M.A. Scott, "Isogeometric fluid–structure interaction analysis with emphasis on non-matching discretizations, and with application to wind turbines", *Computer Methods in Applied Mechanics and Engineering*, Vol. 249–252, 2012, pp. 28-41.

[17] K. Li, X. Qian, "Isogeometric analysis and shape optimization via boundary integral", *Computer-Aided Design*, Vol. 43, No. 11, 2011, pp. 1427-1437.

[18] B. Hassani, S.M. Tavakkoli, N.Z. Moghadam, "Application of isogeometric analysis in structural shape optimization", *Scientia Iranica*, Vol. 18, No. 4, 2011, pp. 846-852.

[19] J. Rots, "Smeared and discrete representations of localized fracture", International Journal of Fracture, Vol. 51, No. 1, 1991, pp. 45-59.

[20] J.C.J. Schellekens, R. De Borst, "On the numerical integration of interface elements", *International Journal for Numerical Methods in Engineering*, Vol. 36, No. 1, 1993, pp. 43-66.

[21] J.C. Simo, J. Oliver, F. Armero, "An analysis of strong discontinuities induced by strain-softening in rate-independent inelastic solids", *Computational Mechanics*, Vol. 12, No. 5, 1993, pp. 277-296.

[22] J. Oliver, "Modelling strong discontinuities in solid mechanics via strain softening constitutive equations. Part 2: Numerical simulation", *International Journal for Numerical Methods in Engineering*, Vol. 39, No. 21, 1996, pp. 3601-3623.

[23] T. Belytschko, T. Black, "Elastic crack growth in finite elements with minimal remeshing", *International Journal for Numerical Methods in Engineering*, Vol. 45, No. 5, 1999, pp. 601-620.

[24] I. Babuška, Z. Zhang, "The partition of unity method for the elastically supported beam", *Computer Methods in Applied Mechanics and Engineering*, Vol. 152, No. 1–2, 1998, pp. 1-18.
[25] I. Babuska, Melenk, J, "The partition of unity method", *International Journal for Numerical Methods in Engineering*, Vol. 40, No., 1997, pp. 727–758.
[26] M.A. Scott, X. Li, T.W. Sederberg, T.J.R. Hughes, "Local refinement of analysis-suitable t-splines", *Computer Methods in Applied Mechanics and Engineering*, Vol. 213–216, 2012, pp. 206-222.
[27] L.A. Piegl, W. Tiller, "The nurbs book", Springer-Verlag GmbH, 1997.
[28] D.F. Rogers, "An introduction to nurbs: With historical perspective", Morgan Kaufmann Publishers, 2001.
[29] M.G. COX, "The numerical evaluation of b-splines", IMA Journal of Applied Mathematics, Vol. 10, No. 2, 1972, pp. 134-149.
[30] C. de Boor, "On calculating with b-splines", Journal of Approximation Theory, Vol. 6, No. 1, 1972, pp. 50-62.
[31] T.W. Sederberg, J. Zheng, A. Bakenov, A. Nasri, "T-splines and t-nurccs", ACM SIGGRAPH 2003 Papers, San Diego, California, 2003, pp. 477-484.
[32] A. Buffa, D. Cho, G. Sangalli, "Linear independence of the t-spline blending functions associated with some particular t-meshes", *Computer Methods in Applied Mechanics and Engineering*, Vol. 199, No. 23–24, 2010, pp. 1437-1445.
[33] A. Buffa, D. Cho, M. Kumar, "Characterization of t-splines with reduced continuity order on t-meshes", *Computer Methods in Applied Mechanics and Engineering*, Vol. 201–204, 2012, pp. 112-126.
[34] M.A. Scott, R.N. Simpson, J.A. Evans, S. Lipton, S.P.A. Bordas, T.J.R. Hughes, et al., "Isogeometric boundary element analysis using unstructured t-splines", *Computer Methods in Applied Mechanics and Engineering*, Vol. 254, 2013, pp. 197-221.
[35] T.W. Sederberg, J. Zheng, A. Bakenov, A. Nasri, "T-splines and t-nurccs", *ACM Trans Graph*, Vol. 22, No. 3, 2003, pp. 477-484.
[36] A. Wang, G. Zhao, Y.-D. Li, "Linear independence of the blending functions of t-splines without multiple knots", *Expert Systems with Applications*, Vol. 41, No. 8, 2014, pp. 3634-3639.
[37] L. Beirão da Veiga, A. Buffa, D. Cho, G. Sangalli, "Isogeometric analysis using t-splines on two-patch geometries", *Computer Methods in Applied Mechanics and Engineering*, Vol. 200, No. 21–22, 2011, pp. 1787-1803.
[38] M.R. Dörfel, B. Jüttler, B. Simeon, "Adaptive isogeometric analysis by local h-refinement with t-splines", *Computer Methods in Applied Mechanics and Engineering*, Vol. 199, No. 5–8, 2010, pp. 264-275.
[39] T.W. Sederberg, D.L. Cardon, G.T. Finnigan, N.S. North, J. Zheng, T. Lyche, "T-spline simplification and local refinement", *ACM Trans Graph*, Vol. 23, No. 3, 2004, pp. 276-283.
[40] E.J. Evans, M.A. Scott, X. Li, D.C. Thomas, "Hierarchical t-splines: Analysis-suitability, bézier extraction, and application as an adaptive basis for isogeometric analysis", *Computer Methods in Applied Mechanics and Engineering*, Vol. 284, 2015, pp. 1-20.
[41] J.-H. Kim, G.H. Paulino, "T-stress, mixed-mode stress intensity factors, and crack initiation angles in functionally graded materials: A unified approach using the interaction integral method", *Computer Methods in Applied Mechanics and Engineering*, Vol. 192, No. 11–12, 2003, pp. 1463-1494.
[42] A. Sutradhar, G.H. Paulino, "Symmetric galerkin boundary element computation of t-stress and stress intensity factors for mixed-mode cracks by the interaction integral method", *Engineering Analysis with Boundary Elements*, Vol. 28, No. 11, 2004, pp. 1335-1350.
[43] R.P. Joseph, J. Purbolaksono, H.L. Liew, S. Ramesh, M. Hamdi, "Stress intensity factors of a corner crack emanating from a pinhole of a solid cylinder", *Engineering Fracture Mechanics*, Vol. 128, 2014, pp. 1-7.
[44] S.N. Bandyopadhyay, H.K. Deysarker, "Stress intensity factor for a crack emanating from the root of a semi-circular edge notch in a tension plate", *Engineering Fracture Mechanics*, Vol. 14, No. 2, 1981, pp. 373-384.
[45] A. Likeb, N. Gubeljak, Y. Matvienko, "Stress intensity factor and limit load solutions for new pipe-ring specimen with axial cracks", *Procedia Materials Science*, Vol. 3, 2014, pp. 1941-1946.
[46] H.-K. Kim, Y.-H. Lee, "Decoupling of generalized mode i and ii stress intensity factors in the complete contact problem of elastically dissimilar materials", *Procedia Materials Science*, Vol. 3, 2014, pp. 245-250.
[47] M. Tur, E. Giner, F.J. Fuenmayor, "A contour integral method to compute the generalized stress intensity factor in complete contacts under sliding conditions", *Tribology*

International, Vol. 39, No. 10, 2006, pp. 1074-1083.

[48] M.L. Williams, "On the stress distribution at the base of a stationary crack.", *ASME Journal of Applied Mechanics*, Vol. 24, No. 1, 1957, pp. 109–114.

[49] S. Mohammadi, "Extended finite element method: For fracture analysis of structures", Wiley, 2008.

[50] E.E. Gdoutos, "Fracture mechanics: An introduction", Springer, 2005.

[51] L. Piegl, W. Tiller, "The NURBS book", U.S. Government Printing Office, 1997.

[52] H. Gómez, V.M. Calo, Y. Bazilevs, T.J.R. Hughes, "Isogeometric analysis of the cahn–hilliard phase-field model", *Computer Methods in Applied Mechanics and Engineering*, Vol. 197, No. 49–50, 2008, pp. 4333-4352.

[53] M. Janssen, J. Zuidema, R. Wanhill, "Fracture mechanics, second edition", Taylor & Francis, 2004.

[54] A.T. Zahnder, "Fracture mechanics", Springer, 2012, p. 234.